Neuromuscular adjustments that constrain submaximal EMG amplitude at task failure of sustained isometric contractions

Jakob L. Dideriksen, Roger M. Enoka and Dario Farina

J Appl Physiol 111:485-494, 2011. First published 19 May 2011;
doi: 10.1152/japplphysiol.00186.2011

J Appl Physiol 111: 485–494, 2011.
First published May 19, 2011; doi:10.1152/japplphysiol.00186.2011.

Neuromuscular adjustments that constrain submaximal EMG amplitude at task failure of sustained isometric contractions

Jakob L. Dideriksen,[1] Roger M. Enoka,[2] and Dario Farina[1,3]

[1]*Center for Sensory-Motor Interaction (SMI), Department of Health Science and Technology, Aalborg University, Aalborg, Denmark;* [2]*Department of Integrative Physiology, University of Colorado, Boulder, Colorado; and* [3]*Department of Neurorehabilitation Engineering, Bernstein Center for Computational Neuroscience, University Medical Center Göttingen, Georg-August University, Göttingen, Germany*

Submitted 10 February 2011; accepted in final form 18 May 2011

Dideriksen JL, Enoka RM, Farina D. Neuromuscular adjustments that constrain submaximal EMG amplitude at task failure of sustained isometric contractions. *J Appl Physiol* 111: 485–494, 2011. First published May 19, 2011; doi:10.1152/japplphysiol.00186.2011.—The amplitude of the surface EMG does not reach the level achieved during a maximal voluntary contraction force at the end of a sustained, submaximal contraction, despite near-maximal levels of voluntary effort. The depression of EMG amplitude may be explained by several neural and muscular adjustments during fatiguing contractions, including decreased net neural drive to the muscle, changes in the shape of the motor unit action potentials, and EMG amplitude cancellation. The changes in these parameters for the entire motor unit pool, however, cannot be measured experimentally. The present study used a computational model to simulate the adjustments during sustained isometric contractions and thereby determine the relative importance of these factors in explaining the submaximal levels of EMG amplitude at task failure. The simulation results indicated that the amount of amplitude cancellation in the simulated EMG (~40%) exhibited a negligible change during the fatiguing contractions. Instead, the main determinant of the submaximal EMG amplitude at task failure was a decrease in muscle activation (number of muscle fiber action potentials), due to a reduction in the net synaptic input to motor neurons, with a lesser contribution from changes in the shape of the motor unit action potentials. Despite the association between the submaximal EMG amplitude and reduced muscle activation, the deficit in EMG amplitude at task failure was not consistently associated with the decrease in neural drive (number of motor unit action potentials) to the muscle. This indicates that the EMG amplitude cannot be used as an index of neural drive.

muscle fatigue; task failure; surface electromyography; first dorsal interosseus; metabolites; neuromuscular modeling

THE AMPLITUDE OF THE SURFACE electromyogram (EMG) depends on the number and amplitude of motor unit action potentials (MUAP) and is often used as an estimate of the neural drive to the muscle (3, 45, 56). When a subject can no longer maintain an isometric contraction at a submaximal target force, however, EMG amplitude does not reach the level achieved during brief maximal voluntary contractions (MVC) performed before the fatiguing contraction (10, 30, 46, 50, 54) despite a voluntary effort that is presumed to be similar in both conditions. The reasons for this discrepancy have not been identified.

Several adjustments during a fatiguing contraction can contribute to the submaximal EMG amplitude at task failure. These adjustments include both those factors that influence motor unit activity and those that modulate the characteristics of the motor unit action potentials in the muscle. As fatigue develops, the motor neuron pool receives less excitatory afferent input due to an increase in feedback transmitted by chemically sensitive type III and IV afferents (9, 31) and a reduction in feedback from stretch-sensitive afferents (19). In addition, the output from the motor cortex may become compromised as the contraction progresses (59). These adjustments in synaptic inputs, possibly combined with changes in intrinsic motor neuron properties (52), are presumably responsible for the gradual decline in motor unit discharge rate that is usually observed during sustained submaximal contractions (8, 10, 13, 32). As these tasks typically require an individual to sustain a target force, the decrease in discharge rate is counterbalanced by the recruitment of additional motor units.

The changes that occur in the muscle during sustained submaximal contractions, such as the accumulation of potassium in the extracellular space, influence both the velocity at which the intracellular action potentials propagate along the muscle fibers (motor unit conduction velocity) and the duration and amplitude of the motor unit action potentials (18, 25, 33, 36, 43). As EMG amplitude corresponds to the sum of motor unit action potentials, changes in the amplitude and duration of motor unit action potentials could influence the summation of the positive and negative phases of the motor unit action potentials (26, 41) and thereby modulate EMG amplitude independent of the output from the spinal cord. Due to technical constraints, it is not possible to measure or systematically control all the parameters that can influence EMG amplitude in experimental conditions. For example, current recording techniques can detect the activity of relatively few motor units, and measurements of conduction velocity are usually only possible for the most superficial motor units. Moreover, the degree of amplitude cancellation is difficult to assess in experimental conditions (11, 26, 41).

The aim of the study was to investigate the relative importance of these factors in explaining the submaximal EMG amplitude at task failure during the simulation of an isometric contraction sustained at a submaximal target force. Similar to a previous study (16), the present study was based on a model of the motor unit activity during sustained isometric contractions (15) that was combined with a model of surface EMG generation (24). The model was expanded in the present study to simulate those adjustments that constrain EMG amplitude at task failure by including antagonist muscle activity and motor unit conduction velocity.

Address for reprint requests and other correspondence: D. Farina, Dept. of Neurorehabilitation Engineering, Bernstein Center for Computational Neuroscience, Univ. Medical Center Göttingen, Georg-August Univ., Von-Siebold-Str. 4, 37075 Göttingen, Germany (e-mail: dario.farina@bccn.uni-goettingen.de).

Table 1. *The parameters used for simulations of motor unit action potentials in the surface EMG model*

Parameter	Assigned Value, mm
Muscle radius	8.67
Mean fiber length	40
Location of innervation zone (from distal tendon attachment)	24
Skin thickness	1.5
Subcutaneous layer thickness	1

METHODS

The model was intended to characterize the first dorsal interosseus muscle (FDI; index finger abductor) and its principal antagonist, the second palmar interosseus (SPI) muscle. The FDI, which comprises ~120 motor units, has been the subject of several previous modeling studies (5, 29), mainly because it is largely responsible for the abduction force exerted by the index finger. The simulated upper limit of motor unit recruitment was set at ~60% MVC force. The proposed model can, however, be adapted to represent other muscles.

Motor unit activity. The model of motor unit recruitment and rate coding and the force exerted by the simulated muscle during fatiguing contractions has been reported previously (15). Therefore, only the main principles of the model relevant to the present study are briefly summarized here. The neural and muscular adjustments during fatiguing contractions were implemented as functions of the metabolite concentration within each muscle fiber and in the extracellular space, using a compartment model approach. Metabolite production was related to the instantaneous muscle activity, and the metabolites were able to diffuse across cell membranes and to be removed in the blood supply. The simulated concentrations were related to the increase in the level of inhibitory afferent feedback, the decline in the amplitude of the twitch force, and the inability of the central nervous system to maintain the target force as fatigue developed. Furthermore, the experimentally observed inability of the motor cortex to produce maximal output during prolonged, sustained contractions (20, 59) was included in the model. Based on these principles, the model was able to simulate experimentally observed trends in parameters, such as time to task failure, changes in recruitment thresholds, trends in motor unit discharge characteristics, and force variability (15).

Antagonistic muscle activity. Besides the increase in agonist EMG amplitude, sustained isometric contractions involve a gradual increase in the EMG amplitude for antagonist muscles (47, 55), which requires a further increase in the agonist muscle activation to maintain the target force. To simulate the contribution of the antagonist muscle to the joint force, the descending drive to the antagonist muscle was increased over time to reproduce trends in EMG (expressed as percentage of MVC amplitude) for the antagonist that were similar to those observed experimentally for the SPI during sustained index finger abduction at target forces of 20 and 60% MVC (47). The resulting antagonist force was subtracted from the simulated FDI force to obtain the net muscle force. The model for SPI corresponded to a scaled-down version of the one for FDI, as SPI has approximately one-half the cross-sectional area of FDI (38).

Motor unit conduction velocity. The simulation of changes in motor unit conduction velocity was added to the model (15) by expanding a previous description of the changes in conduction velocity during fatiguing contractions (16). As motor unit conduction velocity depends on motor unit size (2), discharge rate (51), and the degree of muscle fatigue (25, 33, 36, 43), these factors were incorporated in the simulations. Nishizono et al. (51) described the relation between average motor unit conduction velocity and discharge rate ($MUCV_{DR}$) with the equation:

$$MUCV_{DR}(i,t) = 0.49 \cdot \log\left[DR(i,t)\right] + 2.98 \qquad (1)$$

where DR denotes the instantaneous discharge rate (calculated as the mean value in 500-ms epochs), i represents motor unit number, and t indicates time.

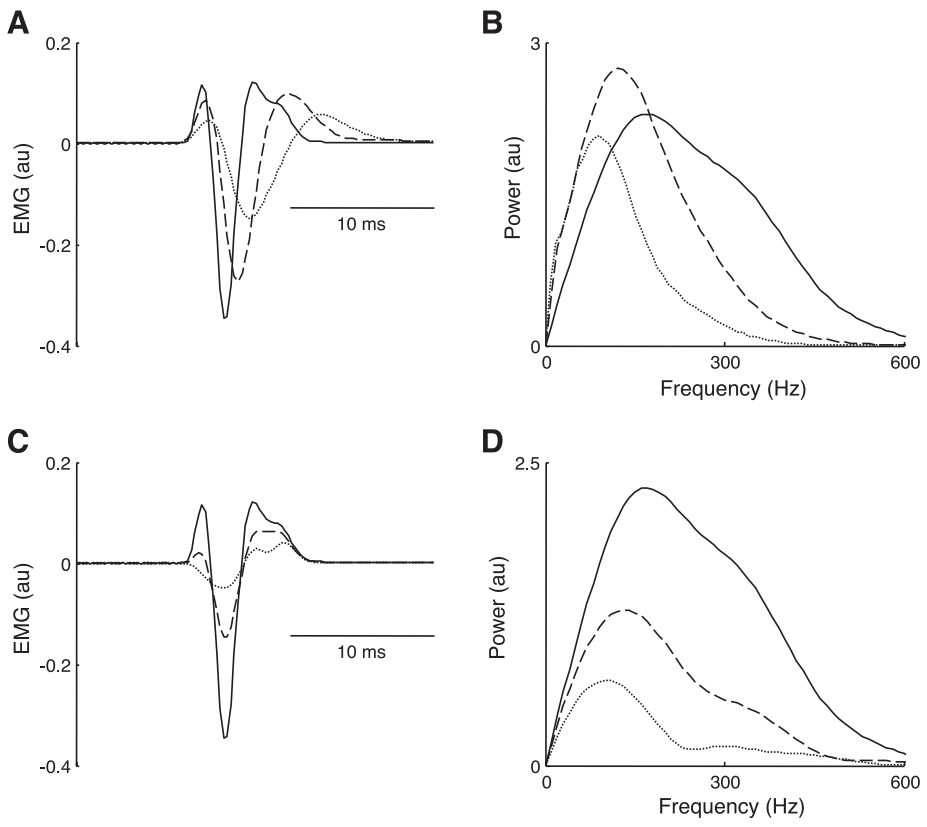

Fig. 1. Simulated motor unit action potentials recorded with surface electrodes for 3 levels of fatigue and different motor unit locations. *A*: influence of fatigue, including no fatigue (motor unit conduction velocity: 4.2 m/s; dark solid line), moderate fatigue (motor unit conduction velocity: 3.5 m/s; dashed line), and severe fatigue (motor unit conduction velocity: 2.2 m/s; light dotted line). *C*: influence of motor unit location, including distances of 5 mm (dark solid line), 10 mm (dashed line), and 15 mm (light dotted line) from the center of the motor unit to the electrode. The motor unit conduction velocity was set to 4.2 m/s for all 3 motor unit action potentials. *B* and *D* indicate the power spectral density for the motor unit action potentials depicted in *A* and *C*, respectively. The time delay from the axis origin in *A* and *C* does not represent the instant of action potential generation. Conversely, the action potentials have been temporally aligned for comparison.

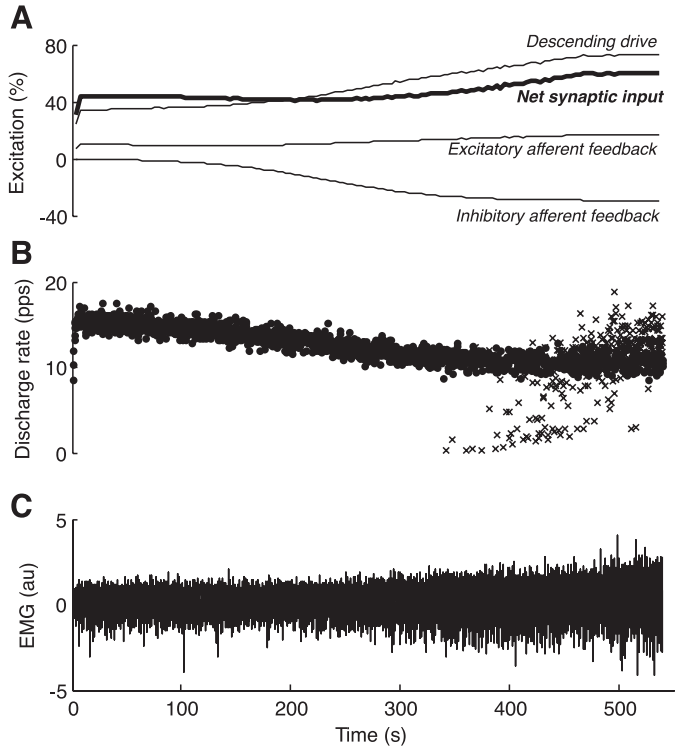

Fig. 2. Synaptic input to a medium sized motor unit (*unit 70*) expressed as a percentage of the maximum level (*A*), the discharge rates for motor *unit 1* (dots) and motor *unit 100* (crosses) (*B*), and the surface EMG (*C*) during the sustained contraction at 20% maximal voluntary contraction (MVC). The net synaptic input (bold line in *A*), which is the sum of the descending drive and the inhibitory and excitatory afferent input, fails to reach the maximum level at task failure. The synaptic input is shown as mean values in 4-s windows, which masks the fluctuations in synaptic noise. Motor *unit 1* exhibited a slight decrease in discharge rate, whereas motor *unit 100* was recruited during the contraction at ~340 s and increased its discharge rate (*B*). The results in *A* and *B* are directly related to the parts of the model described in Ref. 15. au, Arbitrary units.

The dependence of conduction velocity on motor unit size contributes to the distribution of conduction velocity values across the motor unit pool. However, values for the distribution of conduction velocity are difficult to infer from experimental studies. For example, the different results obtained across muscles, such as tibialis anterior (22, 36), vastus medialis and lateralis (25), biceps brachii (43), and abductor pollicis brevis (33), are presumably attributable to differences in fiber-type proportions and average discharge rate, and may be biased by inadequate sampling of the entire motor unit pool. Despite the variability in experimental results, the standard deviation for conduction velocity across motor units is often reported in the range 0.1–0.4 m/s (22, 35, 43). A similar variability can be obtained in simulations by introducing a size dependence in motor unit conduction velocity ($MUCV_{size}$), as described by the following equation:

$$\Delta MUCV_{size}(i) = G_s \cdot (V(i) - \overline{V}) + 1 \quad (2)$$

where G_s denotes the size gain (set to $3.8 \cdot 10^{-3}$), V indicates the motor unit volume (see Equation 1 in Ref. 15), and $\overline{V}$ represents average motor unit volume.

The fatigue-dependent decline in motor unit conduction velocity was related to the simulated extracellular metabolite concentration. Thus the fatigue-induced decline in conduction velocity was similar for all motor units, including those that were not active, as observed experimentally (33, 36, 43). Therefore, motor units recruited during the contraction exhibited an initial conduction velocity that was less than initial values.

The fatigue-dependent decline in conduction velocity is usually observed as an initial linear decline that saturates at ~3 m/s (25, 33, 48). As some of this decline can be explained by a decrease in discharge rate, the direct influence of muscle fatigue on conduction velocity is difficult to estimate. By applying *Eq. 1* to the experimentally observed decline in discharge rate during a 20% MVC contraction sustained for 240 s, as reported by Klaver-Król et al. (43), the expected decline in conduction velocity due to discharge rate alone can be estimated. The difference between this estimated decline and the observed decline in conduction velocity (43) was assumed to be exclusively due to muscle fatigue. With this approach, it was estimated that ~70% of the decline in conduction velocity could be

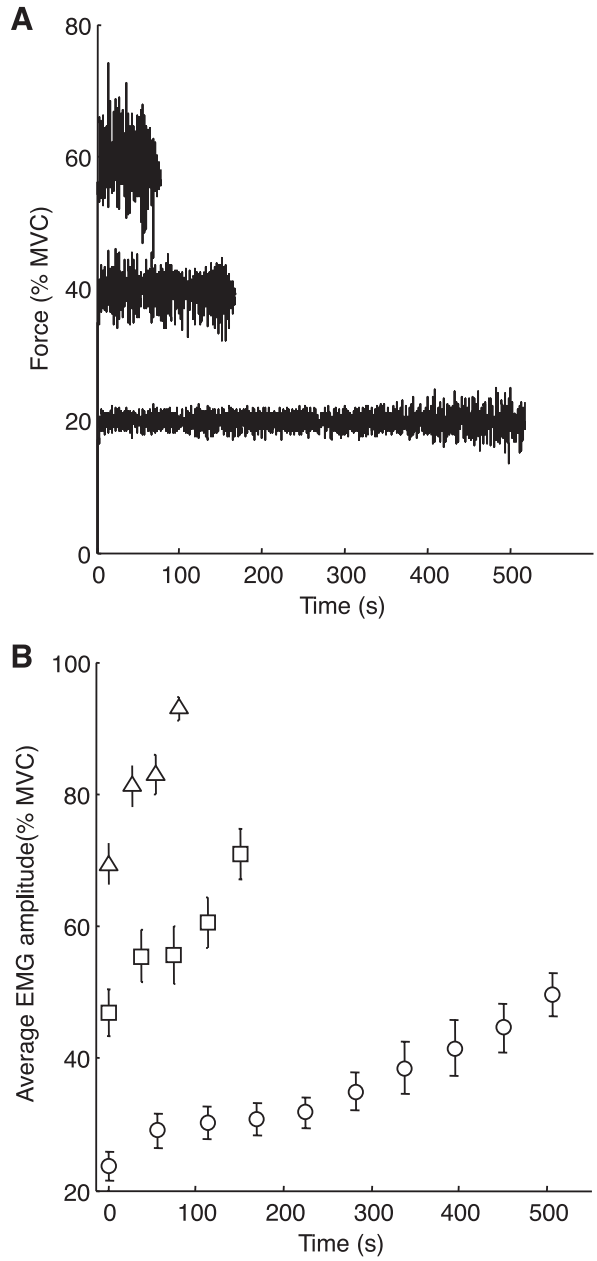

Fig. 3. Force (*A*) and average rectified EMG amplitude (*B*) for the 3 sustained contractions (20, 40, and 60% MVC force). The times to task failure for the contractions at 20%, 40%, and 60% MVC were 520, 190, and 83 s, respectively. The error bars indicate the variability attributable to the 10 different motor unit locations. The results in *A* are directly related to the parts of the model described in Ref. 15.

attributed to the decrease in discharge rate, with the remainder due to muscle fatigue. The size-dependent term (*Eq. 2*) was neglected in this approach as it was assumed that the sample of motor units identified in Ref. 43 was representative of the motor unit population.

Next, the extracellular metabolite concentration was simulated for a 240-s contraction at 20% MVC force with the proposed model to derive a relation between the extracellular metabolite concentration in the model and the decline in conduction velocity due to fatigue. This relation was used to fit the initial slope of a function that declined from 1 to a final value of 0.65 (root mean square error: 0.0027), which corresponded to a minimal value between 2.7 and 3 m/s for motor unit conduction velocity across the motor unit pool, as described by the following equation:

$$\Delta MUCV_{fatigue}(t) = 1 - \tanh\left[\frac{MC_{ES}(t)}{1,200}\right] \cdot 0.35 \quad (3)$$

where MC_{ES} is the simulated extracellular metabolite concentration. Based on *Eqs. 1–3*, the instantaneous motor unit conduction velocities (MUCV) were obtained by the following equation:

$$MUCV(i,t) = MUCV_{DR}(i,t) \cdot \Delta MUCV_{size}(i) \cdot \Delta MUCV_{fatigue}(t) \quad (4)$$

Surface EMG model. The EMG signal was generated using simulations of motor unit action potentials generated by the surface EMG model developed by Farina et al. (24). The model parameters were adopted from a previous modeling study on the FDI (41) and are summarized in Table 1. The modeled muscle tissue was anisotropic and more conductive in the longitudinal fiber direction than in the other directions (anisotropy ratio = 5), whereas the subcutaneous and skin tissues were isotropic. Similar to previous studies (41), the muscle fibers belonging to each MU were modeled in a circular distribution with a mean density of 20 fibers/mm^2. The simulations were achieved with a 4 × 6 mm monopolar electrode that was positioned halfway between the innervation zone and the tendon attachment. Each action potential was simulated 10 times with different randomly assigned locations of the motor unit in the muscle, thereby varying the distance from the source to the electrode to simulate the differences in EMG amplitude observed across subjects in experimental conditions.

The progressive changes in the shape of the intracellular action potentials during the development of fatigue were expanded from the 5 discrete steps described by Dimitrova and Dimitrov (18) to 12 steps by interpolation of the shape parameters. Figure 1, *A* and *B*, depicts a simulated extracellular recording of an action potential for one motor unit and its power spectral density for different degrees of fatigue (*steps 1, 6,* and *12*). Figure 1, *C* and *D*, shows the action potential of the same motor unit at three locations in the muscle (equivalent to three distances from the recording electrodes). Both the amount of fatigue and the distance to the electrode compress the power spectrum and alter the power of the action potential.

Each of the 12 fatigue steps was related to a value for motor unit conduction velocity distributed between 4.8 and 2.7 m/s. A nonlinear distribution between the steps was used (18). As these values were based on observations on low-threshold motor units (34), the size-dependent variability in motor unit conduction velocity (described by Eq. 2) was applied to map the threshold values to motor unit size.

After generating the action potential shapes, the EMG signal was simulated with the model for motor unit activity by summing the action potentials at the discharge times of each active motor unit. To estimate the degree of amplitude cancellation, a second EMG signal was generated in which the action potentials were rectified prior to summation, thereby eliminating the cancellation that occurs when opposite phases are summed. The relation between these two simulated EMG signals indicated the amount of amplitude cancellation (39).

Simulation protocols. Two sets of simulations were performed. The first comprised simulations at target forces of 20, 40, and 60% MVC that were sustained to task failure. The descending drive to the antagonist muscle during the 40% MVC contraction was defined as the mean value between those defined for the 20 and 60% MVC contractions, for which experimental data are available (47). The second set of simulations comprised 30-s ramp contractions (0–100% MVC without antagonist activity) that were repeated several times with different initial values for motor unit conduction velocity. The mean conduction velocity for each simulated ramp was fixed to one value in the physiological range of 2.7 to 5 m/s, with the values distributed around the mean value according to *Eq. 2*. This approach made it possible to obtain the EMG amplitudes that corresponded to all combinations of conduction velocity and muscle activation levels, so that the dependence of EMG amplitude and amplitude cancellation on these two parameters could be derived.

RESULTS

Figure 2 shows the simulated synaptic input for a medium threshold motor unit, the discharge rate of one low- and one high-threshold motor unit (recruitment thresholds <1% MVC and 30% MVC, respectively), and the EMG during a contraction at 20% MVC force. In this example, the descending drive increased throughout the contraction to oppose the change in afferent input and the decrease in the ability of the muscle to produce force. The net synaptic input received by the motor neuron pool failed to reach maximal levels at task failure (Fig. 2*A*). Similar to experimental observations (8, 10, 13, 32, 50), the low-threshold motor unit (*unit 1*) was active throughout the contraction and exhibited a slight decrease in discharge rate, whereas the higher-threshold unit (*unit 100*) was fully recruited during the contraction after a period of ~35 s with sporadic, highly variable discharge times (discharge rate < 2 pps, coefficient of variation for discharge rate > 70%) and from that point exhibited an increase in mean discharge rate over time from ~5 pps to ~14 pps (Fig. 2*B*).

Figure 3 depicts the force traces and the trends in average rectified EMG amplitude (calculated in 10-s epochs) for the contractions sustained at 20, 40, and 60% MVC force. The force variability was within the physiological range for all

Table 2. *Simulation results estimated in 10-s epochs at the beginning of the contraction and at task failure*

	Beginning of Contraction			Task Failure		
	20% MVC	40% MVC	60% MVC	20% MVC	40% MVC	60% MVC
EMG amplitude, % MVC	23.9 ± 2.1	44.3 ± 3.6	68.5 ± 3.1	49.7 ± 2.2	70.1 ± 3.3	92.3 ± 3.4
Motor unit conduction velocity, m/s	4.05 ± 0.05	4.22 ± 0.18	4.33 ± 0.30	3.00 ± 0.29	3.27 ± 0.32	3.67 ± 0.34
Median frequency, Hz	188.8 ± 12.4	201.4 ± 12.7	211 ± 11.3	110.5 ± 8.4	170.0 ± 7.8	187.5 ± 8.1
Amplitude cancellation, %	36.6 ± 4.5	37.3 ± 5.4	38.3 ± 5.4	41.0 ± 5.3	38.9 ± 5.7	38.8 ± 5.1
Antagonist EMG amplitude, %MVC	4.3 ± 0.5	6.5 ± 0.7	10.8 ± 1.4	12.9 ± 1.4	19.4 ± 2.1	28.0 ± 2.4
Antagonist force, % MVC	1.2	2.5	4.9	5.8	11.6	19.5

MVC, maximal voluntary contraction.

contraction levels (15). The EMG amplitude increased over time for all contractions but did not reach the maximal level (Table 2). The error bars in the figure indicate the variability introduced by the 10 motor unit locations. The simulated EMG amplitudes at the beginning of the contraction and at task failure were compared with experimental findings from the FDI (10, 30, 47). A regression analysis indicated a strong linear association for the mean values of the simulated and experimental data at the beginning (Fig. 4*A*, $r^2 = 0.79$) and end (Fig. 4*B*, $r^2 = 0.78$) of the fatiguing contractions. There was a modest linear increase in the antagonist surface EMG amplitude and the force exerted by the antagonist muscle (Table 2).

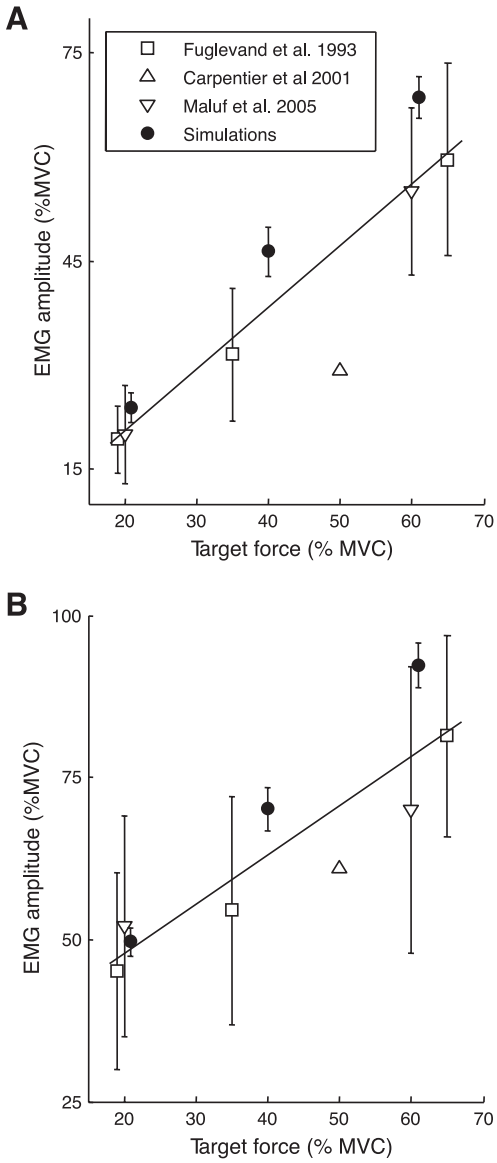

Fig. 4. Relation between EMG amplitude at the beginning of the contraction (*A*) and at task failure (*B*) for each target force as predicted by the model (filled circles) and those reported in 3 experimental studies on the FDI: 2 with sustained isometric contractions (30, 47) and 1 with intermittent isometric contractions (10). The lines indicate the best fit between the experimental and simulated data (*A*: $y = 0.89x + 2.66$, $r^2 = 0.79$; *B*: $y = 0.76x + 32.54$, $r^2 = 0.78$). SDs were not available for the experimental data reported by Carpentier et al. (10).

The median power frequency of the EMG declined linearly for all contraction levels, as observed experimentally (12, 30, 49) (Table 2). The magnitude of the decline for the 20% MVC contraction corresponded well with those observed experimentally for the FDI (30), whereas the simulated declines were smaller than those observed experimentally for the stronger contractions. The values for median power frequency were generally overestimated with respect to experimental observations (30, 43); however, this may be explained by the high sensitivity of this measure to anatomic, physical, and detection-system parameters (23). The initial degree of amplitude cancellation was similar for all contractions (36.5–38.3%) and increased only slightly during the fatiguing contractions, with the greatest increase (~5%) for the 20% MVC contraction (Table 2).

Figure 5 reports the trends in the level of neural drive to the muscle (the number of motor unit action potentials) (Fig. 5*A*) the level of muscle activation (number of muscle fiber discharges) (Fig. 5*B*), and the average conduction velocity for all active motor units (Fig. 5*C*) for the three sustained contractions. After an initial brief increase in the neural drive during all three contractions, the value declined (Fig. 5*A*), mainly due to an increase in inhibitory afferent input. Despite the decline in neural drive, the target force was maintained due to the prolongation of the motor unit twitch contraction time as characterized by the leftward shift of the force-frequency relation (61). The progressive decline in motor unit force, however, eventually required the recruitment of additional motor units when the target force was less than the upper limit of motor unit recruitment (60% MVC force). The gradual recruitment of additional units is reflected as an increase in neural drive for the 20% MVC contraction, but not the 40% MVC contraction (Fig. 5*A*). Despite the decline in the neural drive to the muscle during the contractions at 40% and 60% MVC, the muscle activation level increased (Fig. 5*B*) due to the high innervation numbers of the later recruited motor units. The motor unit conduction velocities declined during the three contractions, but at the fastest rate during the 60% MVC contraction (Fig. 5*C* and Table 2).

Figure 6 shows the relation between the neural drive to the muscle (number of motor unit action potentials) and the muscle activation level (number of muscle fiber action potentials) for different levels of fatigue. The nonlinearity of this relation is attributable to the distribution of innervation number across the motor unit pool with the largest motor unit having the greatest innervation number. As the conditions at task failure for the three contractions involved a decrease in the net synaptic input, neither the neural drive nor the muscle activation level reached the maximal value (nonfatigue curve). The shift of the relation indicates that the contribution of motor units of different size to the total number of motor unit action potentials is redistributed in fatigue. At task failure for the 20% MVC simulation, for example, the maximal effort contraction involved a 30% depression of the neural drive (corresponding to a maximal value of the 20%-MVC curve in Fig. 6 of ~70% of motor unit action potentials) and a 50% decrease in the muscle activation level (muscle fiber action potentials less than 50% of the maximum in the 20%-MVC curve in Fig. 6) relative to the maximal values in nonfatigued condition. Similarly, the neural drive for all other contractions was decreased less than that of the muscle activation level at task failure with respect to nonfa-

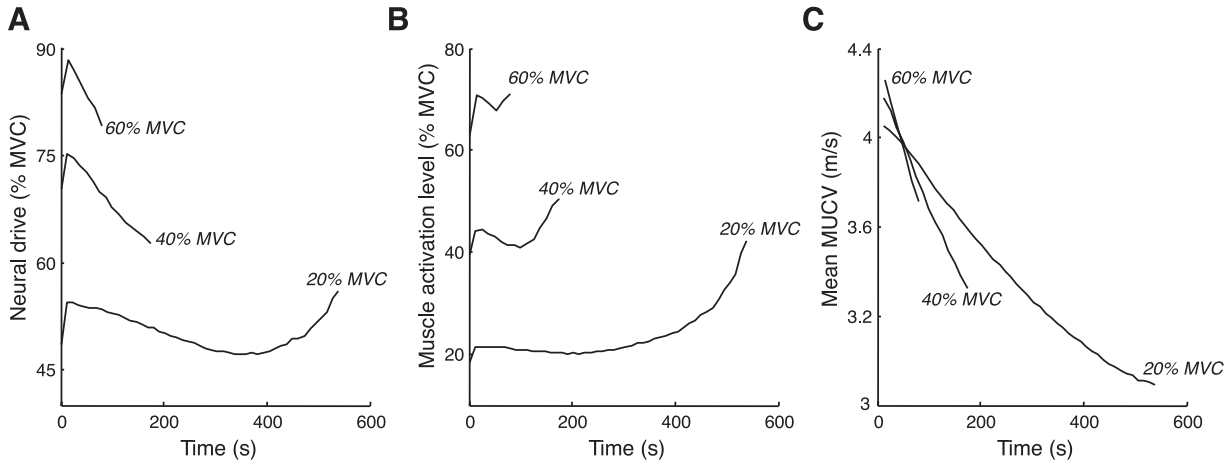

Fig. 5. Neural drive (number of motor unit action potentials) (*A*), muscle activation level (muscle fiber action potentials) (*B*), and average motor unit conduction velocity (*C*) during the 3 sustained contractions. The neural drive and the muscle activation level were normalized to the values obtained during maximal efforts in the absence of fatigue.

tigued condition (maximal values on the horizontal and vertical axes, respectively, of the curves in Fig. 6). This adjustment indicated that motor units with the greatest innervation numbers exhibited the greatest fatigue-related depression in discharge rate. The relations shown in Fig. 6, however, depend on the distribution of innervation numbers across the motor unit pool and likely differ across muscles (21).

Figure 7 indicates the relations between the average rectified EMG amplitude and muscle activation level (number of muscle fiber action potentials) for different values of mean motor unit conduction velocity (2.8, 3.4, 4.0, and 5.0 m/s; each indicating different changes in the intracellular action potential), and between EMG amplitude and mean conduction velocity when varying number of motor unit action potentials (10, 40, 70, and 100% MVC). These associations were derived from the second set of simulations (ramp contractions). The analysis reveals that the muscle activation level was linearly associated with EMG amplitude (Fig. 7*A*), but that the slope of this association depended on conduction velocity. Because the muscle activation level was not linearly related to the neural drive (Fig. 6) and this association was modulated by fatigue, the EMG amplitude was not consistently related to the neural drive (results not shown). As the association between muscle activation level and EMG amplitude was influenced by conduction velocity (Fig. 7*A*), the relation between conduction velocity and EMG amplitude was approximately inversely linear (Fig. 7*B*), as observed experimentally (44), except during severe fatigue (conduction velocity <3.2 m/s). The greatest EMG amplitudes occurred at 3.2–3.3 m/s. Both the muscle activation level and the mean conduction velocity influenced the degree of amplitude cancellation (Fig. 7, *C* and *D*). Amplitude cancellation was not related to the muscle activation level, except at low levels ($<10\%$), and was inversely correlated with mean conduction velocity (39). These results indicate that despite the submaximal EMG amplitude at task failure being mainly due to a decrease in the number of muscle fiber action potentials, neither the muscle activation level nor the neural drive can be consistently inferred from the level of EMG amplitude. The first association is hindered by the dependence of EMG amplitude on conduction velocity (Fig. 7*A*), whereas the second is confounded by the nonlinear relation between number of muscle fiber and motor unit action potentials (Fig. 6).

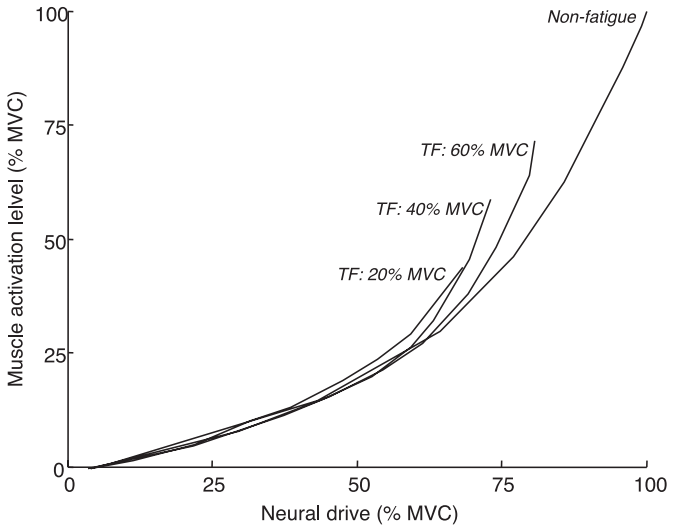

Fig. 6. Relation between neural drive (number of motor unit action potentials) and muscle activation level (number of muscle fiber action potentials) during the simulated ramp contractions in the absence of muscle fatigue (nonfatigue) and in the conditions associated with task failure (TF) for the sustained contractions at 20, 40, and 60% MVC. Fatigue caused a leftward shift of the curve due to the differences in discharge rate experienced by the motor units in the three tasks.

Figure 7 however should be interpreted with caution because it was derived with fixed values of motor unit conduction velocity to simulate all combinations of muscle activation and conduction velocity. As both the muscle activation level and motor unit conduction velocity are depressed at task failure relative to maximal values, not all values of EMG amplitude reported in Fig. 7 correspond to physiologically relevant combinations; for example, the EMG amplitude of $\sim$130% MVC obtained at the maximal level of muscle activation (100%) and mean motor unit conduction velocity of $\sim$3.2 m/s is not feasible because maximal levels of muscle activation can only be achieved in nonfatigued conditions and a conduction velocity of 3.2 m/s denotes severe fatigue.

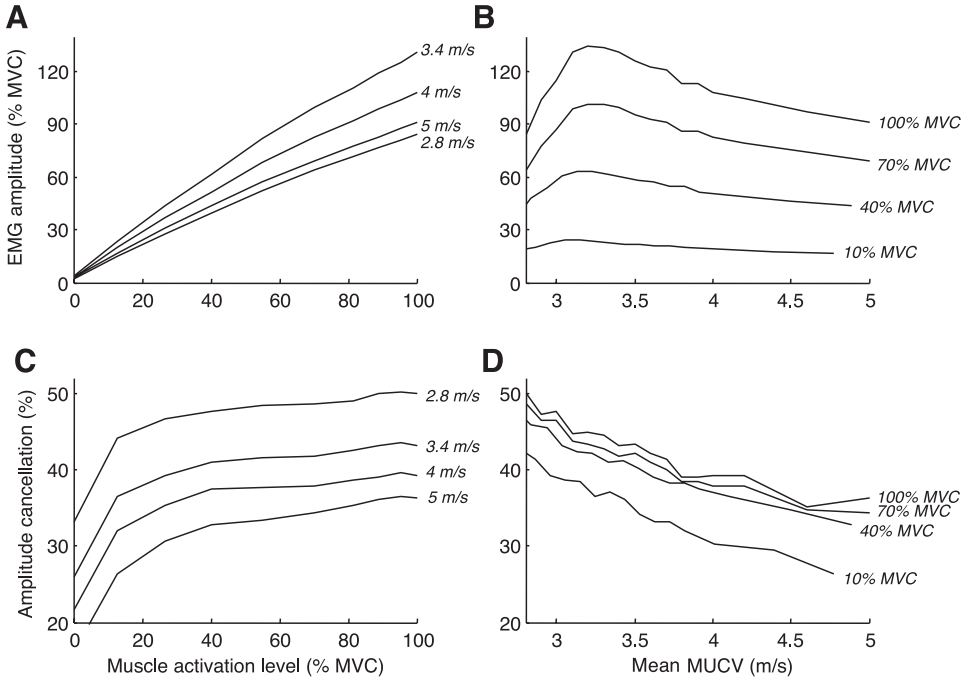

Fig. 7. *A*: derived relations between average rectified EMG amplitude and muscle activation level (number of muscle fiber action potentials). *B*: relations between EMG amplitude and mean motor unit conduction velocity of the active motor units. *C*: relations between EMG amplitude cancellation and muscle activation level. *D*: relations between EMG amplitude cancellation and mean motor unit conduction velocity (MUCV). Each line indicates different levels of mean motor unit conduction velocity (*A, C*) or different levels of muscle activation level (*B, D*). The values of conduction velocity were imposed to simulate the EMG in all combinations of muscle activation (0–100%) and conduction velocity (3–5 m/s). The maxima of the curves in *A* are at lower level conduction velocities for the low levels of muscle activation, since in these cases large motor units (with the highest values of conduction velocity) were not recruited. It is important to note that the entire range of combinations of values of muscle activation level and conduction velocity cannot be achieved experimentally since these are not independent variables.

DISCUSSION

The revised model was able to simulate the amplitude (Fig. 4) and spectral characteristics (Table 2) of the surface EMG during sustained submaximal contractions similar to those observed experimentally (30, 47). Given this capability, the goal of the study was to use the model to identify those neuromuscular adjustments responsible for the depression of EMG amplitude at task failure after sustaining submaximal contractions for as long as possible. Despite the limitations inherent to computational studies, this approach was necessary as it is difficult to distinguish the influence of peripheral and central adjustments during fatiguing contractions experimentally. For example, the synaptic input received by the motor neurons comprises concurrent increases in inhibitory afferent feedback (9, 31) and excitatory descending drive (37, 59). Furthermore, the durations of motor unit action potentials are prolonged during fatiguing contractions, which has opposite effects on EMG amplitude due to increases in the power of each action potential (18) and in the degree of amplitude cancellation (39). Although previous modeling studies have investigated the influence of fatigue-related changes in motor unit action potentials on the EMG amplitude (17, 41, 57), the present study is the first to examine the relative significance of several different adjustments in realistic simulations of isometric contractions at different forces.

In the analysis of the simulation results, a distinction was made between the neural drive to the muscle (quantified by the number of motor unit action potentials) and the level of activation of the muscle induced by the neural drive (quantified by the number of muscle fiber action potentials). These two measures are not equivalent due to the distribution of innervation numbers across the motor unit pool.

The simulations enabled the derivation of theoretical relations between the level of muscle activation and both average motor unit conduction velocity and EMG amplitude (Fig. 7). The linear relation between muscle activation level and EMG amplitude (Fig. 7*A*) and the significant increase in muscle activation during the 20 and 40% MVC contractions (Fig. 5*B*) indicate that the level of muscle activation is the main factor constraining the EMG amplitude at task failure. This interpretation is consistent with the associations between the trends in EMG amplitude (Fig. 3) and the level of muscle activation for the three submaximal contractions (Fig. 5*B*). Based on the parts of the model described previously (15), the results indicated that the inability of the nervous system to increase the level of muscle activation to near-maximal levels was due to a decrease of the net synaptic input to the motor neurons with respect to the maximal input in the absence of fatigue (Fig. 2A).

Despite the simulations suggesting that the EMG amplitude is closely related to the reduction in the level of muscle activation during fatiguing contractions, the depression in the EMG amplitude cannot be used to infer the relative depression in the level of muscle activation because the slope of this association is influenced by changes in conduction velocity (Fig. 7*A*). Moreover, the relation between the magnitude of the deficit in neural drive (the number of motor unit action potentials) and the deficit in EMG amplitude is not consistent due to the nonlinear relation between the neural drive and muscle activation level (Fig. 6). These conclusions are consistent with previous reports (16, 18, 27).

The simulation results showed that the levels of neural drive and muscle activation had different effects on EMG amplitude. The neural drive was nonlinearly related to EMG amplitude due to the exponential distribution of innervation number across the motor unit pool. In contrast, the level of muscle activation was more directly related to EMG amplitude (Fig. 7*A*), although the shapes of the action potentials also influenced this association (Fig. 7*B*). Furthermore, the fatigue-related decline in discharge rate varies with motor unit size (15), which influences the relation between the

number of active motor units and the number of active muscle fibers during the contraction (Fig. 6).

EMG amplitude was also influenced by the changes in the shape of the motor unit action potentials with fatigue, especially in the early stages of the contraction when the level of muscle activation was either stable or decreased (Fig. 5*B*). For example, the increase in EMG amplitude during the 60% contraction (Fig. 3*B*) can only be attributed to changes in the shape of the motor unit action potentials due to the absence of a change in the level of muscle activation (Fig. 5*B*). Close to task failure of the 20% MVC contraction, however, the slow conduction velocities (<3.2 m/s) dampened the decrease in EMG amplitude caused by the significant increase in the level of muscle activation (Fig. 5*B*), due to the nonlinear relation between conduction velocity and EMG amplitude (Fig. 7*B*).

The simulated levels of amplitude cancellation had a negligible influence on these trends as it changed only slightly during the contraction (Table 2), even though previous reportings indicate that significant changes in amplitude cancellation can occur in fatigue (39). Although the simulation results support this finding (Fig. 7, *C* and *D*), the conditions in which amplitude cancellation is maximal were not achieved with the current simulations (20, 40, and 60% MVC).

Limitations of the model. It has been suggested that the submaximal EMG amplitude at task failure could be due to both a decrease in the number of motor unit action potentials and an impairment of neuromuscular propagation (30). However, several experimental studies concluded that neuromuscular propagation is not typically impaired during voluntary fatiguing contractions (7, 42, 58, 60), which is why this phenomenon was not included in the present model. Furthermore, the present results, as well as previous simulation results (40), indicate that even without a deficit in neuromuscular propagation, the EMG amplitude does not reach maximal levels at task failure.

Similarly, EMG amplitude could be modulated by an increase in motor unit short-term synchronization (4, 44, 63), but it is not known how this parameter changes during fatiguing contractions (31). Experimental observations in an intrinsic hand muscle indicate that short-term synchronization increases only slightly during fatiguing contractions (14), and is therefore unlikely to have a substantial influence on the changes in the EMG amplitude. Accordingly, short-term synchronization was not included in the present simulations.

The observation that motor units can be derecruited during sustained contractions (6, 62) was also not included in the present study due to the constraints of the task. As the task was to maintain the target force, the derecruitment of a motor unit would require either the recruitment of another motor unit (6, 62) or an increase in the discharge rate of active motor units thereby largely eliminating the long-term effect on the EMG amplitude. Furthermore, such adjustments have usually only been observed during weak contractions (6, 62) or those that are sustained beyond the task failure (53) and conversely not during moderate contraction levels (1).

As the model equations were based on a large number of experimental observations performed in different conditions and subjects, the simulation results are expected to reflect only general trends and it is not appropriate to compare the results at the level of the individual subject. Although some intersubject variability was introduced by varying the locations of the motor units in the muscle when simulating the EMG, any interpretation beyond general trends should be made with caution. Perhaps the greatest uncertainty of the present study was the model of motor unit conduction velocity. The knowledge in this area is limited, partly due to the technical difficulties related to measuring conduction velocity for the entire motor unit pool. Therefore, the implemented relation between muscle fatigue and decline in motor unit conduction velocity (*Eq. 3*) represents a simplified version of the detailed mechanisms that operate at the level of the fiber membrane. Although more detailed models of the influence of potassium concentration on motor unit conduction velocity have been proposed (28), changes in potassium concentrations and other ions (e.g., calcium) in each muscle fiber and in the extracellular space of the muscle during fatiguing contractions are difficult to describe quantitatively and thus to include in an integrative model.

In conclusion, the simulated results were similar to experimentally observed trends in the surface EMG during sustained, submaximal contractions (Fig. 4). At task failure, the level of muscle activation (the number of muscle fiber action potentials) was depressed due to a decrease in synaptic input relative to the level reached in maximal contractions without fatigue. The decrease in net synaptic input was attributable to a net decrease in the level of afferent feedback and a decline in the capacity of the central nervous system to provide maximal excitation (Fig. 2). In addition to the depression of muscle activation, EMG amplitude was also influenced, although to a lesser extent, by the fatigue-induced changes in the shape of the motor unit action potentials. Despite the influence of the neural drive (number of motor unit action potentials and the level of muscle activation) on EMG amplitude, the depression of EMG amplitude at task failure cannot be used to infer the deficits in either of these parameters.

ACKNOWLEDGMENTS

We acknowledge Martin Bækgaard for his contribution to this study.

DISCLOSURES

No conflicts of interest, financial or otherwise, are declared by the author(s).

REFERENCES

1. **Adam A, De Luca CJ.** Recruitment order of motor units in human vastus lateralis muscle is maintained during fatiguing contractions. *J Neurophysiol* 90: 2919–2927, 2003.
2. **Andreassen S, Arendt-Nielsen L.** Muscle fibre conduction velocity in motor units of the human anterior tibial muscle: a new size principle parameter. *J Physiol* 391: 561–571, 1987.
3. **Ansley L, Schabort E St. Clair Gibson A, Lambert MI, Noakes TD.** Regulation of pacing strategies during successive 4-km time trials. *Med Sci Sports Exerc* 36: 1819–1825, 2004.
4. **Arabadzhiev TI, Dimitrov VG, Dimitrova NA, Dimitrov GV.** Influence of motor unit synchronization on amplitude characteristics of surface and intramuscularly recorded EMG signals. *Eur J Appl Physiol* 108: 227–237, 2010.
5. **Barry BK, Pascoe MA, Jesunathadas M, Enoka RM.** Rate coding is compressed but variability is unaltered for motor units in a hand muscle of old adults. *J Neurophysiol* 97: 3206–3218, 2007.
6. **Bawa P, Pang MY, Olesen KA, Calancie B.** Rotation of motoneurons during prolonged isometric contractions in humans. *J Neurophysiol* 96: 1135–1140, 2006.

7. **Bigland-Ritchie B, Kukulka CG, Lippold OCJ, Woods JJ.** The absence of neuromuscular transmission failure in sustained maximal voluntary contractions. *J Physiol* 330: 265–278, 1982.
8. **Bigland Ritchie B, Johansson R, Lippold OCJ.** Changes in motoneurone firing rates during sustained maximal voluntary contractions. *J Physiol* 340: 335–346, 1983.
9. **Bigland-Ritchie B, Dawson NJ, Johansson RS, Lippold OCJ.** Reflex origin for the slowing of motoneurone firing rates in fatigue of human voluntary contractions. *J Physiol* 379: 451–459, 1986.
10. **Carpentier A, Duchateau J, Hainaut K.** Motor unit behaviour and contractile changes during fatigue in the human first dorsal interosseus. *J Physiol* 534: 903–912, 2001.
11. **Day SJ, Hulliger M.** Experimental simulation of cat electromyogram: Evidence for algebraic summation of motor-unit action-potential trains. *J Neurophysiol* 86: 2144–2158, 2001.
12. **De Luca CJ.** Myoelectrical manifestations of localized muscular fatigue in humans. *Crit Rev Biomed Eng* 11: 251–279, 1984.
13. **De Luca CJ, Foley PJ, Erim Z.** Motor unit control properties in constant-force isometric contractions. *J Neurophysiol* 76: 1503–1516, 1996.
14. **Dideriksen JL, Falla D, Bækgaard M, Mogensen ML, Steimle KL, Farina D.** Comparison between the degree of motor unit short-term synchronization and recurrence quantification analysis of the surface EMG in two human muscles. *Clin Neurophysiol* 120: 2086–2092, 2009.
15. **Dideriksen JL, Farina D, Baekgaard M, Enoka RM.** An integrative model of motor unit activity during sustained submaximal contractions. *J Appl Physiol* 108: 1550–1562, 2010.
16. **Dideriksen JL, Farina D, Enoka RM.** Influence of fatigue on the simulated relation between the amplitude of the surface electromyogram and muscle force. *Philos Transact A Math Phys Eng Sci* 368: 2765–2781, 2010.
17. **Dimitrov GV, Arabadzhiev TI, Hogrel J, Dimitrova NA.** Simulation analysis of interference EMG during fatiguing voluntary contractions. II. Changes in amplitude and spectral characteristics. *J Electromyogr Kinesiol* 18: 35–43, 2008.
18. **Dimitrova NA, Dimitrov GV.** Interpretation of EMG changes with fatigue: Facts, pitfalls, and fallacies. *J Electromyogr Kinesiol* 13: 13–36, 2003.
19. **Duchateau J, Balestra C, Carpentier A, Hainaut K.** Reflex regulation during sustained and intermittent submaximal contractions in humans. *J Physiol* 541: 959–967, 2002.
20. **Eichelberger TD, Bilodeau M.** Central fatigue of the first dorsal interosseous muscle during low-force and high-force sustained submaximal contractions. *Clin Physiol Funct Imaging* 27: 298–304, 2007.
21. **Enoka RM.** *Neuromechanics of Human Movement* (4th ed.). Champaign, IL: Human Kinetics, 2008.
22. **Farina D, Arendt-Nielsen L, Merletti R, Graven-Nielsen T.** Assessment of single motor unit conduction velocity during sustained contractions of the tibialis anterior muscle with advanced spike triggered averaging. *J Neurosci Methods* 115: 1–12, 2002.
23. **Farina D, Cescon C, Merletti R.** Influence of anatomical, physical, and detection-system parameters on surface EMG. *Biol Cybern* 86: 445–456, 2002.
24. **Farina D, Mesin L, Martina S, Merletti R.** A surface EMG generation model with multilayer cylindrical description of the volume conductor. *IEEE Trans Biomed Eng* 51: 415–426, 2004.
25. **Farina D, Pozzo M, Merlo E, Bottin A, Merletti R.** Assessment of average muscle fiber conduction velocity from surface EMG signals during fatiguing dynamic contractions. *IEEE Trans Biomed Eng* 51: 1383–1393, 2004.
26. **Farina D, Cescon C, Negro F, Enoka RM.** Amplitude cancellation of motor-unit action potentials in the surface electromyogram can be estimated with spike-triggered averaging. *J Neurophysiol* 100: 431–440, 2008.
27. **Farina D, Holobar A, Merletti R, Enoka RM.** Decoding the neural drive to muscles from the surface electromyogram. *Clin Neurophysiol* 121: 1616–1623, 2010.
28. **Fortune E, Lowery MM.** The effect of extracellular potassium concentration on muscle fiber conduction velocity examined using model simulation. *Conf Proc IEEE Eng Med Biol Soc* 2007: 2726–2729, 2007.
29. **Fuglevand AJ, Winter DA, Patla AE.** Models of recruitment and rate coding organization in motor-unit pools. *J Neurophysiol* 70: 2470–2488, 1993.
30. **Fuglevand AJ, Zackowski KM, Huey KA, Enoka RM.** Impairment of neuromuscular propagation during human fatiguing contractions at submaximal forces. *J Physiol* 460: 549–572, 1993.
31. **Gandevia SC.** Spinal and supraspinal factors in human muscle fatigue. *Physiol Rev* 81: 1725–1789, 2001.
32. **Garland SJ, Enoka RM, Serrano LP, Robinson GA.** Behavior of motor units in human biceps brachii during a submaximal fatiguing contraction. *J Appl Physiol* 76: 2411–2419, 1994.
33. **Gazzoni M, Camelia F, Farina D.** Conduction velocity of quiescent muscle fibers decreases during sustained contraction. *J Neurophysiol* 94: 387–394, 2005.
34. **Gydikov A, Gatev P, Dimitrov GV, Gerilovsky L.** Changes in the parameters of human single muscle fiber potentials with consecutive discharges. *Exp Neurol* 76: 12–24, 1982.
35. **Hedayatpour N, Arendt-Nielsen L, Farina D.** Motor unit conduction velocity during sustained contraction of the vastus medialis muscle. *Exp Brain Res* 180: 509–516, 2007.
36. **Houtman CJ, Stegeman DF, Van Dijk JP, Zwarts MJ.** Changes in muscle fiber conduction velocity indicate recruitment of distinct motor unit populations. *J Appl Physiol* 95: 1045–1054, 2003.
37. **Hunter SK, Yoon T, Farinella J, Griffith EE, Ng AV.** Time to task failure and muscle activation vary with load type for a submaximal fatiguing contraction with the lower leg. *J Appl Physiol* 105: 463–472, 2008.
38. **Jacobson MD, Raab R, Fazeli BM, Abrams RA, Botte MJ, Lieber RL.** Architectural design of the human intrinsic hand muscles. *J Hand Surg* 17: 804–809, 1992.
39. **Keenan KG, Farina D, Maluf KS, Merletti R, Enoka RM.** Influence of amplitude cancellation on the simulated surface electromyogram. *J Appl Physiol* 98: 120–131, 2005.
40. **Keenan KG, Farina D, Merletti R, Enoka RM.** Influence of motor unit properties on the size of the simulated evoked surface EMG potential. *Exp Brain Res* 169: 37–49, 2006.
41. **Keenan KG, Farina D, Merletti R, Enoka RM.** Amplitude cancellation reduces the size of motor unit potentials averaged from the surface EMG. *J Appl Physiol* 100: 1928–1937, 2006.
42. **Klass M, Guissard N, Duchateau J.** Limiting mechanisms of force production after repetitive dynamic contractions in human triceps surae. *J Appl Physiol* 96: 1516–1521, 2004.
43. **Klaver-Król EG, Henriquez NR, Oosterloo SJ, Klaver P, Bos JM, Zwarts MJ.** Distribution of motor unit potential velocities in short static and prolonged dynamic contractions at low forces: use of the within-subject's skewness and standard deviation variables. *Eur J Appl Physiol* 101: 647–658, 2007.
44. **Kleine BU, Stegeman DF, Mund D, Anders C.** Influence of motoneuron firing synchronization on SEMG characteristics in dependence of electrode position. *J Appl Physiol* 91: 1588–1599, 2001.
45. **Kooistra RD, de Ruiter CJ, de Haan A.** Conventionally assessed voluntary activation does not represent relative voluntary torque production. *Eur J Appl Physiol* 100: 309–320, 2007.
46. **Lind AR, Petrofsky JS.** Amplitude of the surface electromyogram during fatiguing isometric contractions. *Muscle Nerve* 2: 257–264, 1979.
47. **Maluf KS, Shinohara M, Stephenson JL, Enoka RM.** Muscle activation and time to task failure differ with load type and contraction intensity for a human hand muscle. *Exp Brain Res* 167: 165–177, 2005.
48. **Merletti R, Knaflitz M, De Luca CJ.** Myoelectric manifestations of fatigue in voluntary and electrically elicited contractions. *J Appl Physiol* 69: 1810–1820, 1990.
49. **Merletti R, Lo Conte LR.** Surface EMG signal processing during isometric contractions. *J Electromyogr Kinesiol* 7: 241–250, 1997.
50. **Mottram CJ, Jakobi JM, Semmler JG, Enoka RM.** Motor-unit activity differs with load type during a fatiguing contraction. *J Neurophysiol* 93: 1381–1392, 2005.
51. **Nishizono H, Kurata H, Miyashita M.** Muscle fiber conduction velocity related to stimulation rate. *Electroencephalogr Clin Neurophysiol* 72: 529–534, 1989.
52. **Nordstrom MA, Gorman RB, Laouris Y, Spielmann JM, Stuart DG.** Does motoneuron adaptation contribute to muscle fatigue? *Muscle Nerve* 35: 135–158, 2007.
53. **Peters EJD, Fuglevand AJ.** Cessation of human motor unit discharge during sustained maximal voluntary contractions. *Neurosci Lett* 274: 66–70, 1999.

54. **Petrofsky JS, Glaser RM, Phillips CA.** Evaluation of the amplitude and frequency components of the surface EMG as an index of muscle fatigue. *Ergonomics* 25: 213–223, 1982.
55. **Rudroff T, Justice JN, Matthews S, Zuo R, Enoka RM.** Muscle activity differs with load compliance during fatiguing contractions with the knee extensor muscles. *Exp Brain Res* 203: 307–316, 2010.
56. **St. Clair Gibson A, Schabort EJ,Noakes TD.** Reduced neuromuscular activity and force generation during prolonged cycling. *Am J Physiol Regul Integr Comp Physiol* 281: R187–R196, 2001.
57. **Stegeman DF, Linssen WHJP.** Muscle fiber action potential changes and surface EMG: a simulation study. *J Electromyogr Kinesiol* 2: 130–140, 1992.
58. **Taylor JL, Butler JE, Gandevia SC.** Altered responses of human elbow flexors to peripheral-nerve and cortical stimulation during a sustained maximal voluntary contraction. *Exp Brain Res* 127: 108–115, 1999.
59. **Taylor JL, Gandevia SC.** A comparison of central aspects of fatigue in submaximal and maximal voluntary contractions. *J Appl Physiol* 104: 542–550, 2008.
60. **Thomas CK, Woods JJ, Bigland-Ritchie B.** Impulse propagation and muscle activation in long maximal voluntary contractions. *J Appl Physiol* 67: 1835–1842, 1989.
61. **Thomas CK, Johansson RS, Bigland-Ritchie B.** Attempts to physiologically classify human thenar motor units. *J Neurophysiol* 65: 1501–1508, 1991.
62. **Westgaard RH, De Luca CJ.** Motor unit substitution in long-duration contractions of the human trapezius muscle. *J Neurophysiol* 82: 501–504, 1999.
63. **Yao W, Fuglevand AJ, Enoka RM.** Motor-unit synchronization increases EMG amplitude and decreases force steadiness of simulated contractions. *J Neurophysiol* 83: 441–452, 2000.